Aggregation in Living Polymer Solutions by Light and Neutron Scattering: A Study of Model Ionomers

L. J. Fetters,*,† N. P. Balsara,*,‡ J. S. Huang,† H. S. Jeon,‡ K. Almdal,§ and M. Y. Lin†

Corporate Research Laboratories, Exxon Research and Engineering Company, P.O. Box 998, Clinton Township, Annandale, New Jersey 08801-0998, Department of Chemical Engineering, Polytechnic University, Six Metrotech Center, Brooklyn, New York 11201, and Department of Solid State Physics, Risø National Laboratory, P.O. Box 49, Roskilde, Denmark DK-4000

Received February 14, 1995; Revised Manuscript Received May 4, 1995⊗

ABSTRACT: Small angle neutron scattering in combination with dynamic and static light scattering has been used to evaluate the association behavior of the styryl- and dienyllithium head groups in benzene. Both types of lipophobic active centers were found to aggregate as dimers which in turn can self-assemble to yield large scale structures. For the dienyllithium systems no evidence for the presence of tetrameric aggregates was found. The assay of the large scale structures revealed them to be prolate ellipsoids. Thus, these model ionomer systems exhibit diblock copolymer and surfactant style behavior in their capacity to generate cylindrical micelles.

Introduction

Living anionic polymerization of dienes and styrene, based on organolithium compounds, has been of long term academic and commercial interest.[1,2] These reactions are well mastered from a synthetic point of view such that polymers with controlled molar mass, architecture, and narrow molar mass distribution can be made. However, the question of the mechanism through which the chain growth event takes place is not resolved. A key question is the aggregation behavior of the organolithium head groups. Reactions are usually carried out in nonpolar, hydrocarbon solvents such as benzene and cyclohexane. The active centers in such media are, however, prone to self-association due to their ionic character. This could have a substantial effect on the reaction kinetics because chain propagation occurs at these sites. Aggregation numbers of 2 and 4 have been proposed, based mainly on vacuum viscometry[1,3] and on interpretations of propagation kinetics.[2,4–6] While these experiments provide qualitative evidence for aggregation, quantitative interpretations[3–6] are based on assumptions that are today difficult to justify.

In this paper the aggregation behavior of living polymer chains is evaluated using scattering techniques. These chains may be considered as model ionomers with a single lipophobic ionic head group per chain where the extent of ionic character of the carbon–lithium bond appears to be in the vicinity of 85%.[7,8] The association behavior of ionomers are of general interest because of their unique rheological properties in solution.[9] High-vacuum anionic polymerization of hydrogenous styrene was conducted in deuterated benzene, in a specially designed reactor equipped with scattering cells. Scattering samples of the living solutions were isolated by heat-sealing under vacuum. Our approach to the evaluation of head-group association behavior involves small angle neutron scattering (SANS) coupled with light scattering, both static (SLS) and dynamic (DLS). This combination allows the coverage of a large range of scattering vectors, Q, where

$$Q = \frac{4\pi}{\lambda} \sin \frac{\theta}{2} \tag{1}$$

with λ the wavelength of the radiation (light or neutrons) in solution and θ the scattering angle. This joint acquisition of data over a wide Q range is vital, as will be seen, for the elucidation of the structures of the aggregated species. Our results indicate the coexistence of two aggregated species: dimers and rodlike micelles. No evidence for unimers or other aggregates, at detectable concentrations, was found. It will become clear that the aggregation behavior we observe for these anions in a nonpolar solvent is not surprising from an ionomer or surfactant point of view. However, the results have some important consequences for our understanding of the mechanism of lithium-initiated anionic polymerization in hydrocarbon solvents. A section at the end of the paper is devoted to this discussion.

Experimental Section

Living polymer solutions were prepared using established vacuum line protocols.[10] Perdeuterated compounds (benzene, methanol, and the dienes) were obtained from Cambridge Isotopes, Andover, MA. Purified *sec*-butyllithium was used as an initiator, and degassed methanol-d_4 was used as the terminator. Styrene was distilled from dibutylmagnesium into the reactor. This precluded the presence of thermally generated polystyrene. All termination reactions were carried out with near-stoichiometric amounts of methanol (~2:1 ratio of methanol:active center). Two hydrogenous poly(styryllithium) samples in benzene-d_6 were prepared under vacuum. Aliquots of the solutions were terminated for preliminary characterization by size exclusion chromatography (SEC). The molecular weights of the terminated polystyrenes were determined by light scattering and SANS to be 8.6×10^3 and 15×10^3. We refer to the terminated polymers as S(9), SB(9), S(15), and SB(15). Portions of the living solutions—SLi(9) and SLi(15)—were exposed to small amounts of butadiene-d_6 and isoprene-d_8 (~3 diene units per chain end). The diene-capped living polymers are referred to as SBLi and SILi. A four-arm star polymer of S(9) was also synthesized by reacting SBLi(9) with $SiCl_4$. The materials used in this study are summarized in Table 1. A Chromatix KMX-6 instrument was used for the light scattering based molecular weights. Measurements were made on toluene solutions. Polydispersity and star purity were deter-

† Exxon.
‡ Polytechnic University.
§ Risø.
⊗ Abstract published in *Advance ACS Abstracts,* June 1, 1995.

0024-9297/95/2228-4996$09.00/0 © 1995 American Chemical Society

Table 1. Molecular Characteristics of Polystyrene Chains

sample	$10^{-3} M_w$	M_z/M_w[a]	M_w/M_n[a]	f_w[b]
S(9), SLi(9), SBLi(9)	8.6	1.03	1.04	
S(15), SLi(15), SBLi(15), SILi(15)	15.0	1.01	1.02	
PS-star-SB(35)	35.0	1.01	1.02	4.07

[a] Via SEC; column broadening corrections were not made. [b] Star functionality: M_w(star)/M_w(arm)

mined by SEC. The Waters 150 SEC instrument was equipped with two 30 cm and two 60 cm linear Phenomonex Styragel columns; a combination that assures good resolution.

Most of our experiments were conducted on 0.030 and 0.041 g/mL solutions of the 15K and the 9K polystyrene based systems, respectively. These solutions correspond to active center concentrations of 2×10^{-3} and 4.8×10^{-3} M^{-1}. A few experiments were conducted on diluted SBLi(9)/benzene-d_6 solutions. The living solutions were captured in flat quartz cells with a 5 mm path length for the SANS experiments and cylindrical cuvettes with a 12 mm diameter (o.d.) for the light scattering experiments. The scattering cells were attached to the reactor by glass-blowing. Vacuum line integrity was maintained at all times; the scattering samples were isolated by heat-sealing the cells from the reactor. Samples were stored in a freezer (−12 °C) prior to the scattering experiments.

The SANS measurements (20 °C) were done at the National Institute of Science and Technology, Cold Neutron Research Center, in Gaithersburg, MD. The NG-7 30-m spectrometer was used with wavelengths of either 0.6 or 1.3 nm for the incident beam. The wavelength spread $\Delta\lambda/\lambda$ was 14%. The detector distance was selected to yield a Q range of $\cong 6 \times 10^{-2}$ to 1 nm^{-1}. A position sensitive two-dimensional detector was used. Due to the azimuthal symmetry of the SANS scattering pattern, the data were azimuthally averaged in order to improve the signal to noise ratio. The pure deuterated solvent was measured separately to allow for the subtraction of the incoherent scattering. The 15K series was used in two separate runs which varied in the Q range covered. Both data sets are presented.

Static and dynamic light scattering experiments were performed on an ALV-5000 instrument, using an argon ion laser (λ = 632.8 nm) as the light source. Data were obtained at scattering angles between 30 and 150°. The temperature was maintained at 25.0 ± 0.2 °C with the exception where temperatures were cycled to 55 °C. The SLS signals were converted to absolute intensities using pure toluene as a secondary standard. The absolute calibration was verified by measuring Rayleigh ratios of other solvents such as cyclohexane. The angular independence of the measured scattering from these low molecular weight solvents was also used to verify alignment of the instrument.

The autocorrelation function of the scattered intensity, $g(\tau)$, was accumulated in the homodyne mode and used to obtain the intensity-weighted distribution of mobilities, $G(\Gamma)$, by solving the following integral equation:[11]

$$g(\tau) = B[\alpha\{\int_0^\infty G(\Gamma) \exp(-\Gamma\tau)\, d\Gamma\}^2 + 1] \qquad (2)$$

The solution for the above was obtained using CONTIN, a software package developed by Provencher.[12]

Literature data available only in figures were reclaimed via the use of the Un-Plot-It automated digitizing system (Silk Scientific, Inc.).

Results

SANS. The SANS measurements were done on the base poly(styryllithium) (Table 1), the diene-capped counterparts, the terminated species, and the four-arm star. Figure 1 shows the Q dependence of intensity, $I(Q)$, for the terminated SB(9), the living SBLi(9), and the four-arm star SB(35). The respective intercepts demonstrate that a 2-fold difference in molecular weight

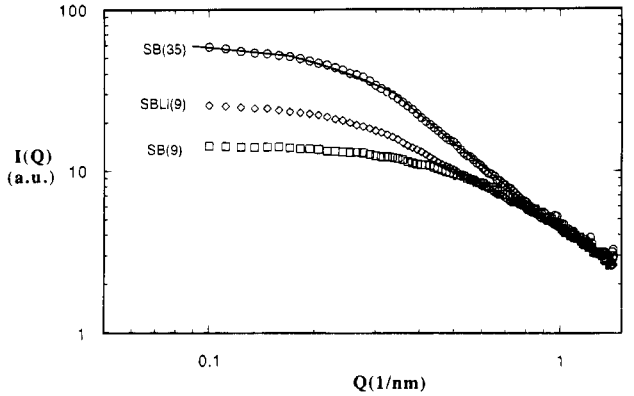

Figure 1. Scattering intensity, $I(Q)$, for terminated SB(9), SBLi(9), and four-armed SB(35). The solid line is the simulation result. $I(Q)$ is in arbitrary units.

holds for SB(9) and SBLi(9) and that a 4-fold difference exists when the four-arm star is compared with the parent arm. The measured radii of gyration, R_G, of 2.6 nm SB(9), 3.7 nm SBLi(9), and 4.5 nm SB(35) are in good agreement with those predicted[13,14] for the singlet (2.6 nm), dimer (3.8 nm), and star (4.3 nm). It is clear from these parallel comparisons that aggregated tetrameric structures are not present in detectable concentrations (the lower limit of detectability is ca. 10%).

The simulation approach of Grest[15] fortifies the conclusion regarding the absence (or near absence) of the aggregated tetramer structure. Figure 1 shows the SB(35) scattering data coupled with the simulation results (solid line). The experimental and simulated four-arm star profiles coincide and are clearly different from that of SBLi(9), the head group of which is claimed[4] to exclusively yield the tetrameric structure.

Figure 2a shows the SB(15) scattering profile, $S(Q)$, as a function of scattering vector, Q. The radius of gyration obtained by Guinier analysis, 3.2 nm, is in good agreement with the calculated[13] value of 3.4 nm.

Figure 2b–d shows the scattering behavior of SLi(15), SBLi(15), and SILi(15). At low Q (Q < 0.1 nm^{-1}) it is apparent that an upswing in the scattering intensity is observed. This behavior is a manifestation of the presence of the dimer in coexistence with larger scale species. Furthermore the SLi(15), SBLi(15), and the SILi(15) show nearly identical structure factors in the Q regime of ~1–0.1 nm^{-1}, which demonstrates that the association states of the small scale aggregates are *identical*, i.e., dimeric. The R_G values obtained by eliminating the low Q data are about 5.4 nm for SLi(15), SBLi(15), and SILi(15) and agree well with the projected[13] value of 5.6 nm for the dimer. The low Q data lead to *apparent* R_G values of 14.9 nm for SILi(15), 16.3 nm for SLi(15), and 20.2 nm for SBLi(15). An example of the method used to derive these values is given in Figure 3. These values may be contrasted with the projected R_G of 6.5 nm for a four-armed star, having 1.5×10^4 g mol^{-1} arms.[13,14] As has been found, arm stretching is absent for low-functionality stars.[16–19] Thus, the apparent R_G values cannot be taken as an indication that "stretched-arm" tetramers are present in the dienyllithium-capped systems. The *apparent* R_G values, however, indicate the presence of larger scale structures of sufficient size so as to be outside the limits of the SANS Q range.

The SANS measurements have shown that dimers are present in these active living systems and that they coexist with larger scale aggregates having functional-

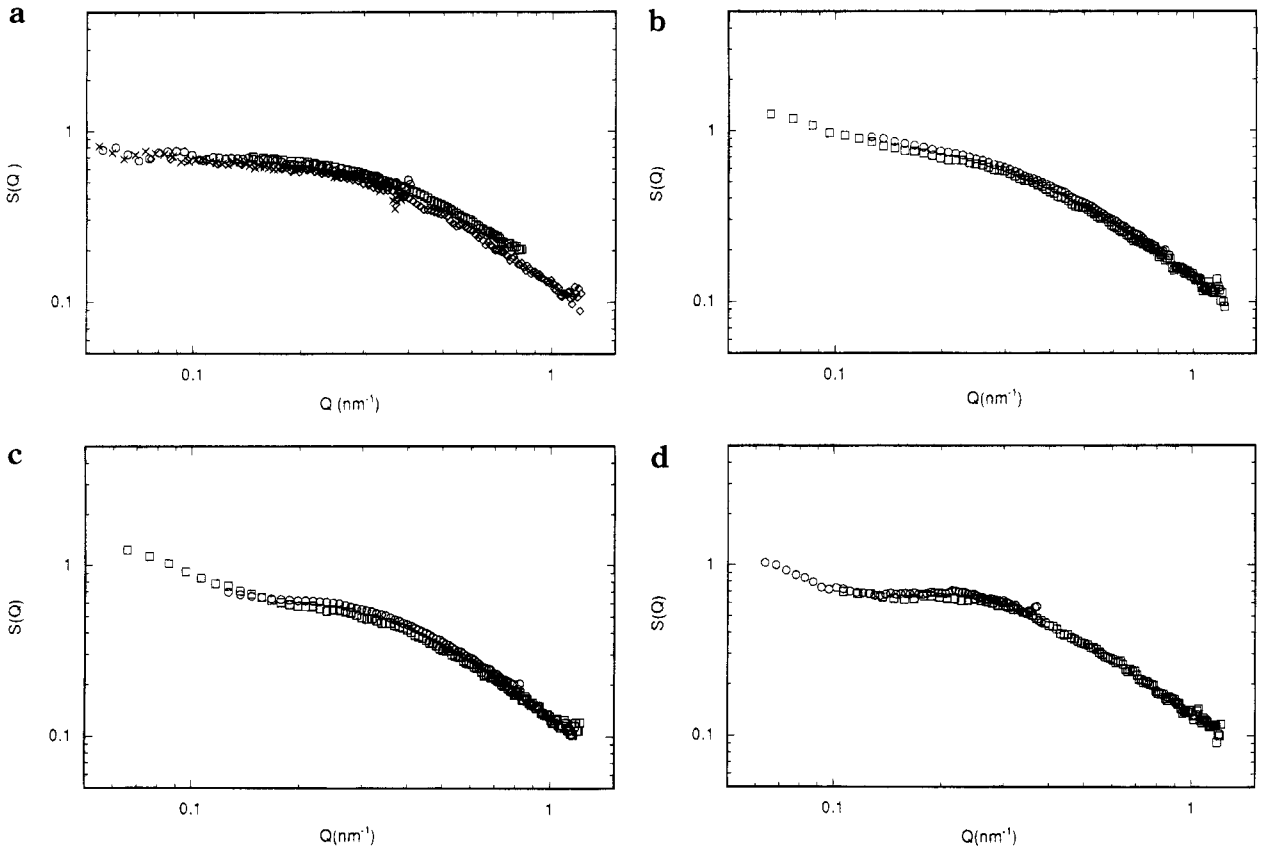

Figure 2. (a) Structure factor for terminated SB(15): units for $S(Q)$ are cm^{-1}. (b) Structures factor for SLi(15). (c) Structure factor for SBLi(15). (d) Structure factor for SILi(15).

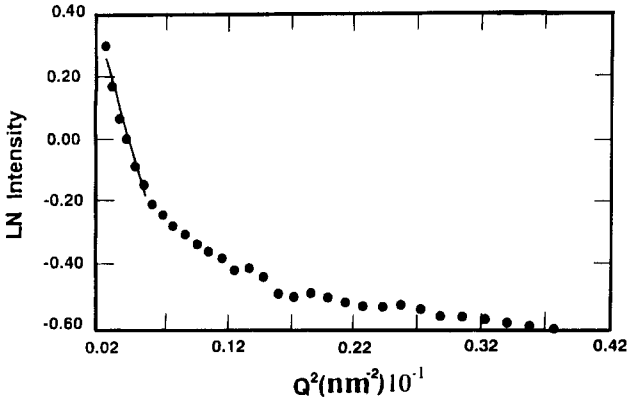

Figure 3. Evaluation of apparent R_G via low Q SANS data for SBLi(15).

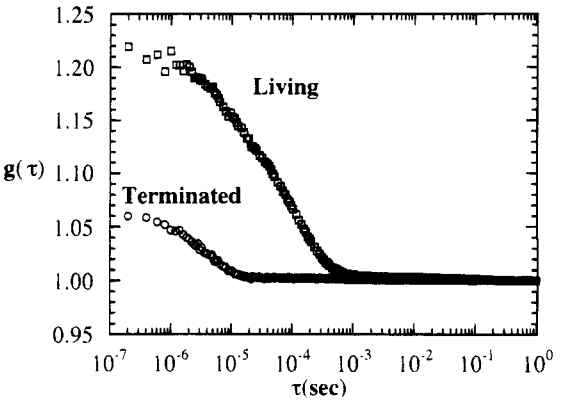

Figure 4. Intensity correlation function, $g(\tau)$, vs time for terminated and associating chains: SB(15) and SBLi(15).

ities well beyond that of 4. Thus, it was necessary to access lower Q regions (larger wavelengths) in order to identify the architecture *and* size of those species. This was done via SLS and DLS.

Static and Dynamic Light Scattering. In Figure 4 we compare DLS signals obtained from the SBLi(15) solution (c = 0.03 g/mL) before and after termination. Both autocorrelation curves were obtained at the scattering angle of 90°; [$Q = 2.73 \times 10^{-2}$ mm^{-1}]. It is evident that the characteristic relaxation time of the living solution is 2 orders of magnitude longer than that of the terminated solution. This confirms the presence of large aggregates in the living solutions. At this juncture it should be mentioned that the deactivated solutions were collected, after termination, from the master solution from which the living systems were captured. This protocol eliminated the possibility that scattering impurities, e.g., dust, were present in the living polymer solutions and absent in their terminated counterparts.

The distribution of mobilities obtained from the terminated SBLi(15) solution, SB(15), is shown in Figures 5a. A single peak dominates this distribution. The characteristic decay rate associated with a relaxation mode, Γ_c, is assumed to be equal to the ratio of the first and zeroth moments of the peak. In Figure 5b we show the dependence of Γ_c on Q. The relaxation mode is diffusive—$\Gamma_c \sim Q^2$; the diffusion coefficient associated with this relaxation mode, D, is given by the slope of the Γ_c versus Q^2 plot and is equal to 1.05×10^{-6} cm^2/s. The Stokes–Einstein relationship can be used to estimate the hydrodynamic radius of the diffusing species, R_h:

$$D = kT/6\pi\eta R_h \qquad (3)$$

where k is the Boltzmann constant, T is absolute

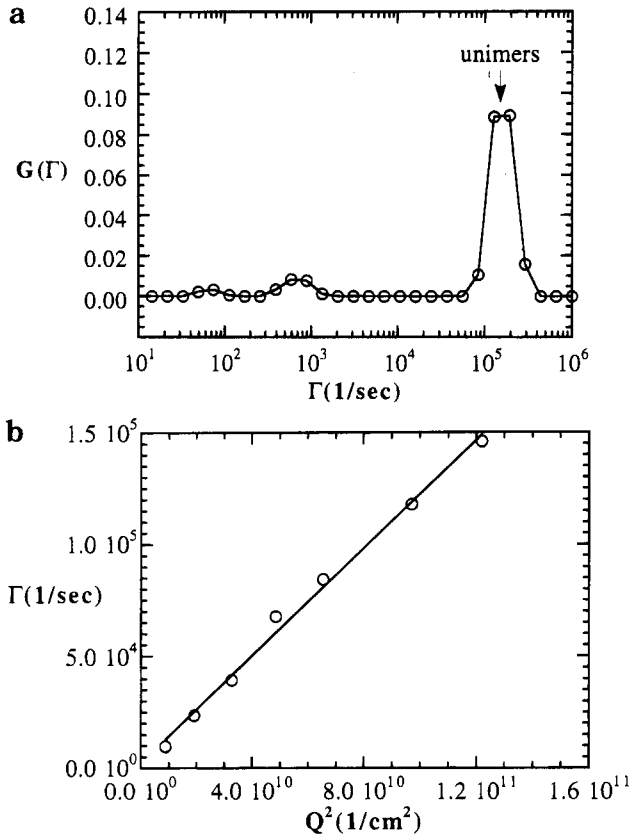

Figure 5. (a) Intensity weighted distributions of mobility obtained from the terminated SBLi(15) solution. (b) Dependence of Γ_c on Q^2.

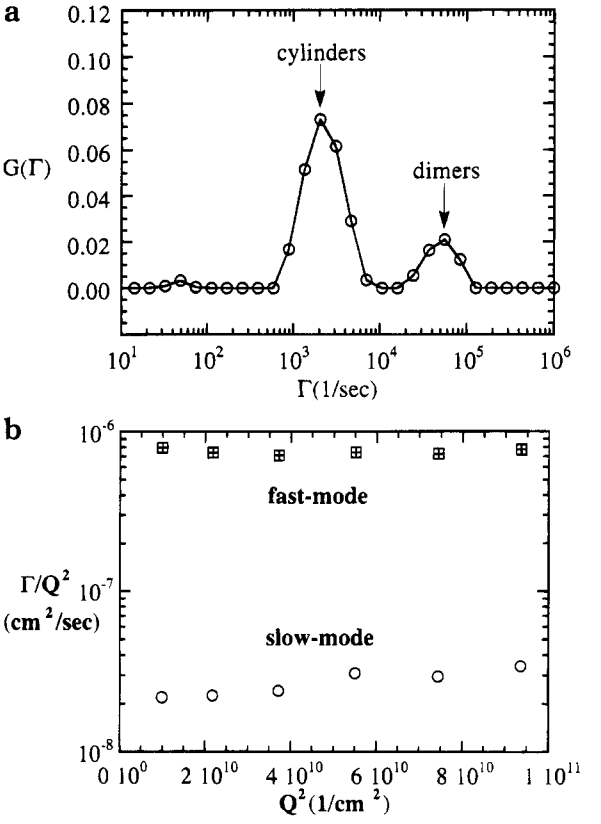

Figure 6. (a) Intensity weighted distributions of mobility obtained from the SBLi(15) solution. (b) Dependence of Γ_{cs} and Γ_{cf} on Q^2 for the SBLi(15) solution.

temperature, and η is the viscosity of the solvent. The value of R_h for the terminated chain is 3.45 ± 0.31 nm. According to Huber et al.[20] R_h of PS ($M_W = 1.5 \times 10^4$) in benzene (at 22 °C) is 3.3 nm. The measured R_h from the terminated solution is thus within experimental error of that expected from individual chains.

The distribution of mobilities obtained from the living SBLi(15) solution ($c = 0.03$ g mL^{-1}, $Q = 2.73 \times 10^{-2}$ nm^{-1}) is shown in Figure 6a. A fast mode with a characteristic decay rate of $\Gamma_{cf} = 6.49 \times 10^4$ (1/s) and a dominant slow mode with a decay rate of $\Gamma_{cs} = 2.12 \times 10^3$ (1/s) were found. The dominant fast and slow modes account for 87% of the DLS measured distribution of mobilities.

In Figure 6b we show the dependence of Γ_{cs} and Γ_{cf} on Q. Both relaxation modes are diffusive. At low angles (below 45°) the slow mode accounts for more than 95% of the distribution of mobilities. Thus at the lower angles, only the slow mode could be identified. The diffusion coefficient associated with the fast mode is 9.90 $\times 10^{-7}$ cm^2/s, with a corresponding $R_{hf} = 3.66 \pm 0.25$ nm. The presence of the slow relaxation mode affects the accuracy with which the R_{hf} can be determined. The expected R_h of the dimer is 4.6 nm.[13] The SANS measurements are therefore ideally suited for determining the presence of the more rapidly diffusing species; the dimers.

The diffusion coefficient associated with the slow mode is 3.26×10^{-8} cm^2/s, with a corresponding $R_{hs} = 111.1 \pm 15.0$ nm. This value is considerably larger than the size of dimers or tetramers. The fully extended length of the SBLi(15) molecule is 18.0 nm. The fact that the measured R_h in benzene is significantly greater than 36.0 nm rules out the possibility of inflated spherical aggregates with lithium cores. We therefore consider other possible structures such as cylindrical micelles. The foregoing conclusion is in agreement with that based on the low Q ($<1 \times 10^{-2}$ nm) SANS results for SBLi(15).

We consider two kinds of structures: a rodlike micelle wherein the head groups are aggregated along the center line and a disklike micelle where the head groups form a two-dimensional planar structure. These aggregates may be approximated as prolate and oblate ellipsoids, respectively. The ellipsoids are obtained by rotating an ellipse with semi-axes a and b about the b axis. The minor semi-axis of the proposed aggregates is restricted to molecular dimensions, and thus must lie between 3.4 and 18 nm (size of the individual chains in toluene and fully extended contour length, respectively). Micelles formed by block copolymers are relatively well understood and chains that comprise the corona of these aggregates are stretched by a factor of 4–5, relative to their unperturbed dimensions.[21,22] Similar behavior is observed for polymer brushes attached to a substrate.[23–25] Using these results, we expect the minor semi-axis to be about 15 nm. The major semi-axis of prolate and oblate ellipsoids that would yield and $R_h = 111$ nm can be calculated from the theory of Perrin.[26,27] Equations 4 and 5 apply to ellipsoids obtained by revolving an ellipse with semi-axes a and b about the a axis.

$$R_h(\text{prolate}) = \frac{a(1 - b^2/a^2)^{1/2}}{\ln\left[\frac{1 + (1 - b^2/a^2)^{1/2}}{b/a}\right]} \qquad a > b \quad (4)$$

$$R_h(\text{oblate}) = \frac{a(b^2/a^2 - 1)^{1/2}}{\tan^{-1}[(b^2/a^2 - 1)^{1/2}]} \qquad a < b \quad (5)$$

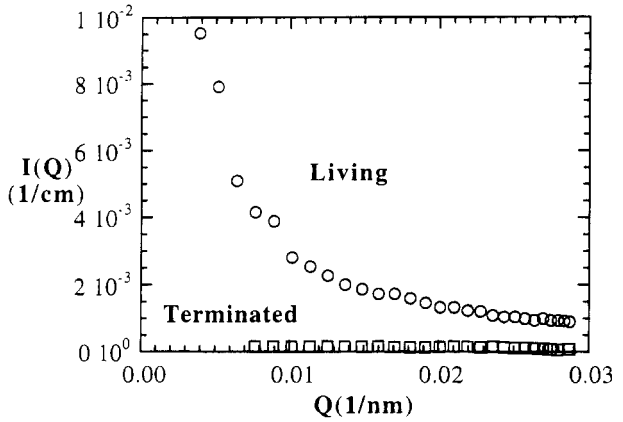

Figure 7. SLS absolute scattered intensity vs Q for the living and terminated versions of SBLi(15).

Table 2. Dimensions of Ellipsoidal Particles Based on a Hydrodynamic Radius of 111.1 nm

minor semi-axis (nm)	major semi-axis (nm)		radius of sphere (nm)
	prolate	oblate	
5	608	172	
10	505	169	
15	466	166	
20	409	161	
25	382	159	
			111.1

The results of these calculations are summarized in Table 2. For completeness we also include the degenerate case obtained for a sphere ($b/a = 1$). All the structures listed in Table 2 are consistent with the DLS data. The static scattering function of these structures, $I(Q)$, can be computed exactly, using classical optics. The most probable structure is determined by comparing experimentally measured SLS data with the computed profiles. In Figure 7 we show the absolute scattered intensity $I(Q)$ versus Q from living and terminated solutions of SBLi(15). The strong positive curvature in $I(Q)$ obtained from the living solution is consistent with the presence of large aggregates. In comparison, the $I(Q)$ obtained form the terminated solution is nearly Q-independent, as expected for free SB(15) chains in the Q range. These data also indicate that the lower limit for the number of chains per aggregate is 10^2. Note that the actual aggregation number would be substantially larger, since one has to extrapolate the data in Figure 7 to $Q = 0$.

The Q dependence of the scattered intensity from the ellipsoidal structures listed in Table 1 were computed, and the results are shown in Figure 8. The curves are normalized scattering curves from a solution containing randomly oriented ellipsoids which can be computed from the following equations:[28]

$$I(Q) = \frac{9\pi}{2}\int_0^{\pi/2}\frac{[J_{3/2}(u)]^2}{u^3}\cos\beta\, d\beta \qquad (6)$$

where $J_{3/2}(u)$ is the $^3/_2$ order Bessel function:

$$J_{3/2}(u) = \left(\frac{2u}{\pi}\right)^{1/2}\left(\frac{\sin u}{u^2} - \frac{\cos u}{u}\right) \qquad (7)$$

and

$$u = qa\left(\cos^2\beta + \frac{b^2}{a^2}\sin^2\beta\right)^{1/2} \qquad (8)$$

The scattering data (SLS) obtained from the SBLi-(15) solution are also shown in Figure 8 which shows

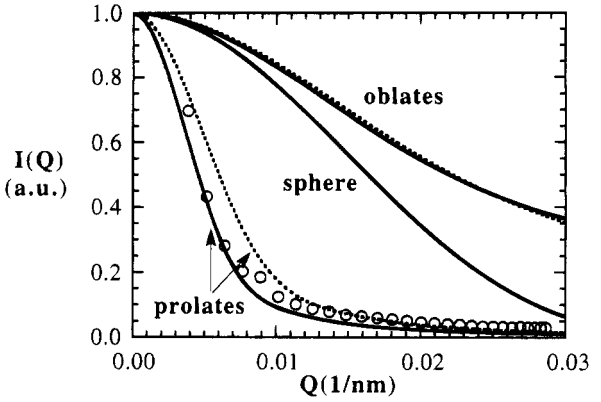

Figure 8. Comparison of experimental SLS data and theoretical calculations for ellipsoids with $R_h = 111$ nm (see Table 2). Solid curves: oblate ellipsoid with $a = 25$ nm and $b = 159$ nm; prolate ellipsoid with $a = 382$ nm and $b = 25$ nm. Dashed curves: oblate ellipsoid with $a = 5$ nm and $b = 172$ nm; prolate ellipsoid with $a = 608$ nm and $b = 5$ nm. Sphere with $a = b = 111$ nm. Symbols represent data for SBLi(15).

the Q dependence of the scattered intensity, $I(Q)$. The experimental data were multiplied by a constant to force agreement between theory and experiment at low scattering angles. We find *near-quantitative* consistency between experiment and theory for the case of prolate ellipsoids. On the other hand, spherical and disklike micelles are *qualitatively* inconsistent with the data. Note that spherical (starlike) micelles are ruled out on the basis of the fully extended length of the chains. Prolate ellipsoids, i.e., rodlike structure, are thus the only structures that are consistent with *both* the static and dynamic light scattering data. We thus conclude that the micelles are rodlike with length $L \approx 800$ nm and diameter $d \approx 30$ nm. A more accurate description of the Brownian motion of rodlike entities was provided by Broersma.[29,30] Applying this theory with $R_h = 111$ nm and $d = 30$ nm, we obtain $L \approx 740$ nm.

It is important to note that the actual micellar structure is quite likely far more intricate than the models that have been considered. We have assumed that the micelles can be approximated as uniform, rigid bodies. The micelle, however, is very likely to have some flexibility. Furthermore, the no-slip boundary condition used by Perrin to derive the expressions for R_h may not be valid because of the presence of mobile polystyrene chains at the particle–solvent interface. Since QL is not much less than 1, it is possible that the DLS signal contains contributions due to rotation and other internal modes available to the aggregate.[31]

We examined several other living solutions and found similar results. Solutions of SILi(15) and SBLi(15) ($c = 0.03$ g mL^{-1}) and solutions of SBLi(9) ($c = 0.0052$, 0.01 and 0.02 g mL^{-1}) exhibited fast and slow modes that were similar to that described above. The DLS results from these solutions are summarized in Figure 9. In all cases the dimers, assayed by SANS, coexisted with large aggregates. The examination of the SILi and SBLi solutions was straightforward because they were colorless. The SLi solutions had the characteristic yellow color, and thus *quantitative* SLS is not possible due to optical absorption. Therefore, we performed DLS experiments on these solutions and observed correlation functions similar to those obtained from the colorless living solutions (Figure 6). The R_h value obtained for the slow mode in SLi(9) was about 700 nm.

In Figure 10 we show the Q dependence of the fraction of the DLS signal attributable to the large aggregates,

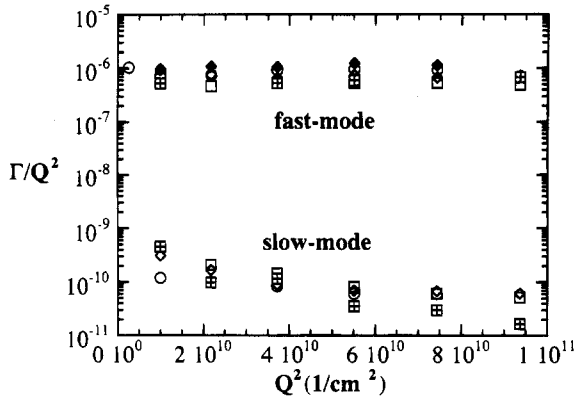

Figure 9. Dependence of Γ_{cs} and Γ_{cf} on Q for SILi(15) (○) (c 0.03 g mL^{-1}), SBLi(15) (♦) (c = 0.03 g mL^{-1}), and SBLi(9) (◇) (c = 0.02 g mL^{-1}), (□) (c = 0.01 g mL^{-1}), (⊞) (c = 0.0052 g mL^{-1}).

ζ.

$$\zeta = \frac{\text{area under cylinder peak}}{\text{area under cylinder peak + area under dimer peak}} \quad (9)$$

If we assume that the solution consists of noninteracting particles, then the area under a given peak at a given Q is proportional to the product of concentration of the species i (c_i) and its static scattering function $S(Q)$.[11] Thus,

$$1/\zeta(Q) = 1 + [c_{dimer}/c_{cylinder}][S_{dimer}(Q)/S_{cylinder}(Q)] \quad (10)$$

Since $S_{cylinder}(Q) \gg S_{dimer}(Q)$ and $S_{dimer}(Q) \approx 2S_{unimer}(Q)$ in the low QR_g limit, the data given in Figures 4 and 10a can be used to estimate the relative amount of chains in the cylindrical format. The ratio of static scattering intensities in terminated and living solutions, $\sigma(Q)$, is given by

$$\sigma(Q) = I_{terminated}(Q)/I_{living}(Q) \approx [1/2][S_{dimer}(Q)/S_{cylinder}(Q)] \quad (11)$$

and

$$1/\zeta(Q) = 1 + 2[c_{dimer}/c_{cylinder}]\,\sigma(Q) \quad (12)$$

In Figure 10b we plot $1/\zeta(Q)$ versus $\sigma(Q)$ for SBLi(15) and find that the data can be represented by a straight line. The slope of the least-squares, linear fit is 1.644. Thus

$$c_{dimer}/c_{cylinder} = 0.822 \quad (13)$$

i.e. 55% of the chains are in the cylindrical form. Note that $\zeta(Q)$ and $\sigma(Q)$ are obtained from *independent* experiments over a range of scattering vectors. Also, the experimentally obtained intercept of 0.986 is in good agreement with the theoretical expectation of 1.0. These facts enhance our confidence in our estimate of the relative concentrations of dimers and cylinder. The length scale probed by SANS is considerably shorter (of the order of 1 nm) than that of SLS. Thus, we expect in the region of $Q \sim 1$ nm^{-1} all polymer segments, irrespective of aggregation state, will contribute to the measured neutron scattering intensity; which depends only on the total concentration of monomers, as seen, for example, in Figure 1. The approach presented here has also been used[32] to study the effect of hydrogen bonding on micelle formation in block copolymers.

Discussion

Aggregation in Related Systems. The aggregation behavior we have observed in the living solutions is not

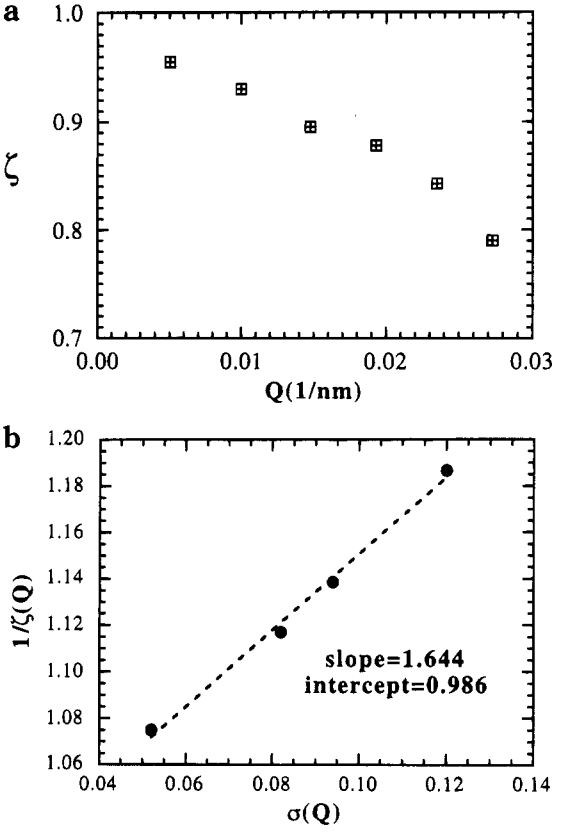

Figure 10. (a) Q dependence of DLS signal attributable to the cylindrical structure, ζ. (b) A plot of $1/\zeta(Q)$ for the SBLi(15) solution. The line represents the least-squares fit through the data, and the relative concentrations of dimers and large scale cylinders can be estimated from the slope of the line. Approximately 55% of the living chains are contained in the large scale aggregates.

completely surprising due to the ionomeric character of the chains. In many respects these chains are similar to the monocarboxylic terminated polystyrenes studied by Jalal and Duplessix.[33] SANS and small angle X-ray scattering demonstrated[33] that those chains formed prolate ellipsoid structures below and above c^*, the overlap concentration of the nonfunctionalized chains. Parallel behavior is also observed in aqueous surfactant systems, e.g., sodium dodecyl sulfate.[34] Those micelles were characterized as rodlike structures with spherical caps at each end. Thus, the cylindrical model is clearly feasible as a large scale structure for species with self-assembling head groups. Nonionic surfactants behave similarly. Cylindrical micelles of alkyl poly(ethylene oxide) in aqueous solution[35] and polystyrene-*block*-poly(*p*-hydroxystyrene) in toluene[32] have been observed. Aggregation numbers of 2 × 10^3 and 1 × 10^4 chains/micelle were reported, while the block polymer micelle showed a length of 300 nm.[32]

Recent evaluations[36] of surfactant organization in micellar systems have demonstrated that the equilibrium structure can consist of wormlike micelles which are much longer than an appropriately defined Kuhn length. Such species have thus been treated theoretically as polymeric. Theory[37] suggests that under appropriate conditions there may be no upper limit to the length of such cylindrical micelles.

Allyllithium is known to be associated in diethyl ether with aggregation states strongly dependent upon concentration.[38,39] Measured association states were found to range from 2 to ca. 14. Hydrocarbon insolubility precludes such measurements although allyllithium is

known to form extended structures in the solid state.[40-42] Furthermore, variable-temperature NMR and cryoscopy have established[43] that allyllithium can form dimers in tetrahydrofuran.

The foregoing demonstrates the capacity of the allyllithium head group to self-assemble in various types of solvents. It is also worth noting that solid state polymeric structures are formed by [*bis*(trimethylsilyl)methyl]lithium.[44] The structure formed involves the methylene carbon bridged between two lithium atoms. Variable aggregation states for oligomeric butadienyllithium in cycloalkanes have also been inferred from ^{13}C NMR studies.[45] As summarized by Weiss,[7] lithium compounds offer the largest structural diversity found in organometallics: "monomers, dimers (rings), trimers (rings), tetramers (heterocubanes and rings), hexamers (pseudooctrahedra), decamers, dodecamers (stacked rings), and polymers (chains, double chains)". The lipophobic head groups examined in this work show that both dimers and polymeric (cylindrical) structures can coexist.

Excluded volume (entropic) and enthalpic considerations combine, along with head-group interactions, to control the large scale aggregate architecture.[46] On the basis of enthalpic considerations alone (see following paragraph) the aggregation numbers are expected to be large. However, interchain repulsions—excluded volume interactions and random thermal fluctuations—can serve to limit aggregate size. These repulsions would be expected[46] to be smallest in a star-shaped (spherical) aggregate, intermediate for a cylindrical (rodlike) aggregate, and largest for a disk. Head-group attractive interactions, based on what is understood[40-42] regarding the solid state packing of allyllithium, seemingly favor the cylindrical structure. As found by Brédas, Chance, and Silbey,[46] the cylindrical structure will maximize attractive energy without sacrificing too much in repulsive energies.

The large scale aggregates examined by us failed to show any detectable decrease in R_h, for SBLi(15) as temperature was cycled from 25 to 55 °C. This suggests that the enthalpic contribution to the aggregation process is large; a conclusion fortified by the size of the large scale structures. *Ab initio* calculations[47] for allyllithium led to a bridged structure for the dimeric state, with an apparent dissociation enthalpy of ca. 172 kJ per dimer, a value in reasonable accord with that of 155 kJ determined[3] for the dimer of poly(isoprenyllithium). This latter value is also that of the *ab initio* calculated[48] dimerization enthalpy of dilithiomethane. Methyl- and ethyllithium yield respectively values of 186 (*ab initio*)[49] and 144 kJ (PRDDO).[50] These values for the dissociation enthalpy are compatible with the currently accepted view[7,8] regarding the highly ionic character of these head groups.[51] As was previously recognized, enthalpies of the foregoing magnitude will lead to an increased aggregate lifetime.[52,53] Figure 11 shows the *ab initio* based[47] bridged structure for the butadienyllithium dimer.

Implication for the Mechanism of Anionic Polymerization. Consider a reaction where a compound, C, in a solution is consumed by a reaction which involves another species, A, present in the solution at constant concentration. This description fits, e.g., monomers in living anionic polymerization. From general chemical kinetics it is easy to show[54] that if the reaction mechanism for the disappearance of C is the reaction sequence

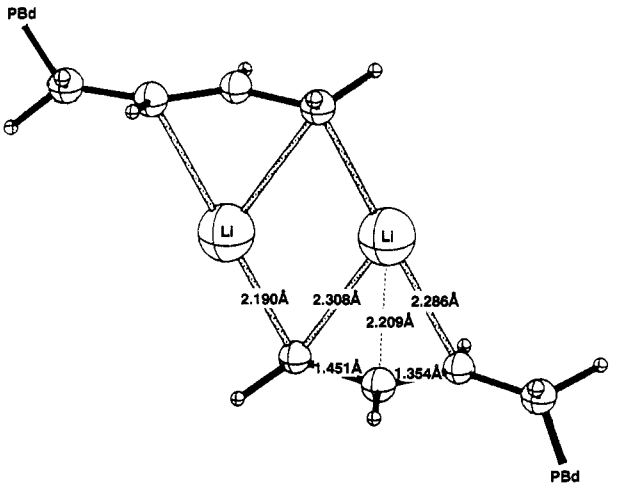

Figure 11. Bridged dimer for the butadienyllithium head group.[47] This structure is adopted from that of allyllithium: Figure 2 of ref 47.

$$A \rightleftharpoons nB$$

fast equilibrium with equilibrium constant K_d

$$B + C \rightarrow B^*$$

rate determining step with rate constant, k

then the rate of disappearance is given by

$$-d[C]/dt = kK_d^{1/n}[A]^{1/n}[C] \qquad (14)$$

Conversely, it is tempting to assume that when a species is observed to have a reaction order less than 1 then this is due to fast reactions preceding the rate determining step. A fractional reaction order can thus be taken as an indication of fast dissociation equilibria preceding the rate determining step. However, it is usually possible to suggest several reaction mechanisms that will lead to the same experimentally observed kinetic expression. Such an exercise was done by Brown, for organolithium based initiation, in 1965.[55] Thus observed kinetics cannot *alone* be taken as a proof of a reaction mechanism. In the long standing debate over the mechanism of anionic polymerization the observation of fractional reaction orders of the living chain has been used as a method of evaluating the association state of the living chain end. This evaluation assumes a reaction mechanism of the above type where A is presumed to be unreactive. In effect, this mechanism subscribes to the validity of the premise that propagation kinetic orders *directly* yield structural information.[6] Other than the dictate of kinetic convenience, no explanation is available as to why aggregation must cause unreactivity. Over time, these assumptions have rather acquired the status of axiom.

Table 3 presents the propagation rate behavior for dienes and styrene monomers in hydrocarbon solvents.[56-72] In terms of eq 14 k denotes the rate constant for the propagation event while the gradient is the slope of the log–log plot of the $-d[C]/dt$:active center concentration. The dienes show gradients ranging from 0.11 to 0.48 (and larger). The 0.48 slope for the isoprene–benzene system was rationalized[63] on the grounds that the predominant aggregates were dimers while at high active center concentration (gradient of 0.18) tetramers were invoked. These observations, coupled with spectroscopic[63] and SLS results,[4,73] led to the conclusion[2,63,74] that the isoprenyllithium head group formed a weaker tetrameric aggregate than the corresponding butadi-

Table 3. Propagation Power Laws for Diene and Styrene Monomers in Hydrocarbons

	monomer	solvent[a]	temp (°C)	10^2k ($M^{-\alpha}$ min^{-1})	gradient α	active center range	ref
PBdLi	butadiene	cyc–hept	30	0.672	0.13	1.3×10^{-2}–1.5×10^{-3}	56, 57
		cyc–hept	30	1.30	0.24	1.2×10^{-3}–5.0×10^{-5}	56, 57
		hex	30	0.650	0.18	1.5×10^{-2}–2.8×10^{-3}	58
		hex	30	1.04	0.26	2.8×10^{-3}–2.2×10^{-4}	58
		hept	−10	*b*	*b*	6.6×10^{-2}–5.2×10^{-5}	59
	styrene	tol	20	0.0647	0.26	9.6×10^{-2}–4.0×10^{-3}	60
		tol	20	0.207	0.46	4.0×10^{-3}–6.9×10^{-5}	60
		cyc[c]	40	0.0584	0.13	1.0×10^{-3}–1.2×10^{-4}	61
PILi	isoprene	ben.	30	6.25	0.20	3.3×10^{-2}–1.2×10^{-3}	58, 62
		ben.	30	14.0	0.32	1.2×10^{-3}:3.4×10^{-4}	58, 62
		ben.	30	6.25	0.18	9.6×10^{-3}–2.7×10^{-4}	63
		ben.	30	79.8	0.48	9.7×10^{-5}–1.5×10^{-6}	63
		hept	20	1.22	0.21	6.0×10^{-2}–8.0×10^{-4}	64
		hept	20	*d*	*d*	8.0×10^{-4}–6.0×10^{-7}	64
		cyc	25	2.26	0.18	2.0×10^{-2}–1.4×10^{-3}	65
		cyc	30	6.03	0.25	1.0×10^{-2}–1.0×10^{-4}	58
		cyc	30	3.67	0.21	1.6×10^{-2}–3.1×10^{-5}	66
		hex	30	3.94	0.23	1.9×10^{-2}–5.5×10^{-4}	58
		hex	30	3.02	0.24	3.9×10^{-3}–6.7×10^{-5}	62
		hex	30	3.32	0.26[e]	6.7×10^{-3}–2.7×10^{-5}	67
		cyc	40	11.7	0.18	8.3×10^{-3}–3.6×10^{-5}	68
		cyc	50	18.0	0.11	2.2×10^{-2}–1.8×10^{-3}	65
		hept	−10	*b*	*b*	5.9×10^{-2}–2.5×10^{-5}	59
	styrene	cyc	40	1.74	0.29	9.9×10^{-3}–1.4×10^{-4}	68
PSLi	styrene	tol	20	107.0	0.67	1.5×10^{-2}–1.2×10^{-4}	69
		cyc	25	52.7	0.56	8.2×10^{-3}–6.3×10^{-5}	70
		tol	30	192.0	0.65	4.0×10^{-2}–5.1×10^{-5}	60
		ben	30	73.1	0.48	4.5×10^{-2}–1.6×10^{-5}	58, 71
		cyc	40	180.3	0.57	9.5×10^{-4}–2.3×10^{-5}	56
		cyc	40	123.0	0.48	1.4×10^{-3}–3.3×10^{-5}	68
	butadiene	tol	25	30180	0.63	1.4×10^{-2}–3.3×10^{-4}	60
		tol[f]	25	38900	0.68	1.6×10^{-2}–1.0×10^{-3}	60
	isoprene	cyc	40	3060	0.50	1.3×10^{-3}–9.0×10^{-5}	68
PMSLi	*o*-methoxystyrene	tol	20	172.0	0.62	1.8×10^{-2}–5.3×10^{-4}	72
		tol	0	90.4	0.80	1.9×10^{-2}–1.4×10^{-3}	72
		tol	−19	24.6	0.87	1.9×10^{-2}–1.4×10^{-3}	72

[a] Cyc = cyclohexane; hex = *n*-hexane; hept = *n*-heptane; ben. = benzene; tol = toluene. [b] Gradient ranged from 0.20 to 0.45. [c] Butadiene present: $[Bd]_0 > [Sty]_0$. [d] Variable increasing gradients with decreasing rate: 0.21 to ca. 2.0. [e] This work utilized a difunctional lithium initiator derived from 1,2-bis(4-isopropenylphenyl)ethane. Over the active center range of 2.9×10^{-4} to 2.7×10^{-5} M^{-1} the gradient ranged from 0.24 to ca. 1. The gradients observed depended on the chain length of the isoprenyldilithium "seed" with the shorter chain (DP = 25) yielding the gradient of about 1. [f] PBdLi present: $[PBdLi]_0/[PSLi]_0 = 1-18$.

enyllithium species. In contrast to that assessment are the Ohlinger–Bandermann findings[60] for the reaction of styrene with butadienyllithium (20 °C). It is seen that the gradient of 0.46 commences at an active center concentration of ca. 4×10^{-3} M^{-1} while the parallel behavior for the isoprene–benzene (30 °C) system occurs at a concentration of about 10^{-4} M^{-1}. Those combined results highlight the inadequacies present in the assumptions upon which the mechanism of eq 14 is predicated. The variability of the gradient as a function of active center concentration is not limited to aromatic solvents. In some cases in alkanes the active centers based on butadiene[56–59] and isoprene[59,63] show increasing values for the respective gradient as active center concentration decreases.

The rate:active center findings for the isoprene–alkane systems are given in Table 3. Although many of these systems show the orthodox gradient of ~0.25, obvious inconsistencies in rates are apparent, i.e., contrary indications are present as to the influence of solvent identity and reaction temperatures.

The *o*-methoxystyrene results[72] show an *increase* in gradient with decreasing temperature. The increase in gradient[72] with decreasing temperature cannot be reconciled with the mechanism that requires aggregate dormancy and the fact that kinetic order reflects the association state. Thus, the gradients (Table 3 and footnote *d*) which range from 0.11 to ~2 do not, as commonly believed, directly reflect the aggregation state of play of the chain ends since the dimer is the primary structure (coupled with the presence of the large scale cylinders) for both styrene and diene systems.

The apparent aggregation state of 4 has been favored by those[2,4,5,63,66,74–85] who embrace the dual conjecture of aggregate dormancy and the fact that propagation kinetics constitute a measure of the association state. Our experiments demonstrate that the aggregation behavior of these living polymer solutions is more complicated than conclusions based on propagation kinetics. This, in turn, seemingly demonstrates that aggregates are reactive in their own right, an event for which evidence and suggestions are available.[52,53,86–89]

Generally, the potential for the existence of aggregation states other than dimers and tetramers has not been considered. A noteworthy exception to this is contained in the 1966 results of Makowski and Lynn.[89] Therein they reported that the bulk viscosity of oligomeric (DP ≃ 6) butadienyllithium differed from its terminated counterpart by the nearly constant factor of 6×10^3 over the temperature range 20–65 °C. The viscosity ratio was found[89] to decrease as the chain length increased. Such behavior is not explainable by the presence of dimers and/or high functionality star-shaped structures[90] but is in consonance with the presence of extended long-range structures where aggregate size is related to chain length.

The methods used to study aggregation behavior have examined systems devoid of monomer. Conversely, by necessity, the kinetic data emerge from systems wherein monomer is the interacting partner of the reactive head groups in the chain growth event. Thus, these two types of analysis unavoidably probe different situations. The large scale structures could conceivably be formed only at or near the end of the polymerization. However, this is an unlikely event due to the following considerations. First, the formation of large scale aggregates is driven by the fact that the ionic head groups at the living chain ends are surrounded by nonpolar moieties. The monomers examined in this study—styrene, isoprene, and butadiene—are also nonpolar. We expect no qualitative changes in the thermodynamic driving force for aggregation as the monomers are consumed. Second, the aggregation tendency is expected to decrease with increasing molecular weight; thus larger aggregates may actually be formed during the initial and intermediate stages of polymerization.[91] Since we find no evidence for the existence of unimers in solution, we are led to the conclusion that aggregated head groups *must be reactive*. We plan to address these issues directly by conducting scattering experiments during polymerization.

Conclusion

The combination of SANS, DLS, and SLS has shown that the aggregation behavior of living polymer chains with the styryl- and dienyllithium head groups[92] is more complicated than previously envisaged. The primary aggregated structure is the dimer.[93] Roughly half of that population self-assembles to yield large scale cylindrical structures. Such aggregation behavior cannot be inferred from measurements of propagation kinetic orders (Table 3) (and, conversely, propagation kinetic orders cannot be inferred from aggregation behavior). The aggregation states of the cylinders would be expected to depend on chain length and, perhaps, to a lesser extent, concentration. The growth of the chain may cause a concurrent decrease in aggregate functionality. The notion that kinetic orders and aggregation states need be directly related is incorrect, at least for the systems studied in this work. Makowski and Lynn recognized[89] the potential of the highly associated structures to complicate the kinetics of initiation and propagation. The role of aggregation in the reaction behavior of these systems is recognizable and thus requires further study.

Acknowledgment. The work of N.P.B. and H.S.J. was supported by the National Science Foundation through Grant No. CTS-9308164, Grant No. DMR-9307098, and the NSF Young Investigator Program, Grant No. DMR-9457950. We also wish to thank a reviewer for several comments which led to a significant change in the paper.

References and Notes

(1) Young, R N.; Quirk, R. P.; Fetters, L. J. *Adv. Polym. Sci.* **1984**, *56*, 1.
(2) van Beylen, M.; Bywater, S.; Smets, G.; Szwarc, M.; Worsfold, D. J. *Adv. Polym. Sci.* **1988**, *86*, 87.
(3) Morton, M.; Fetters, L. J. *J. Polym. Sci., Part A* **1964**, *2*, 3331. Morton, M.; Fetters, L. J.; Bostick, E. E. *J. Polym. Sci., Part C* **1963**, *1*, 311.
(4) Worsfold, D. J.; Bywater, S. *Macromolecules* **1972**, *5*, 393.
(5) Szwarc, M. *Macromolecules* **1994**, *27*, 6221. Fontanille, M.; Helary, G.; Szwarc, M. *Macromolecules* **1988**, *21*, 1532. Laita, Z.; Szwarc, M. *Macromolecules* **1969**, *2*, 412. Yamagishi, A.; Szwarc, M.; Tung, L.; Lo, G. Y.-S. *Macromolecules* **1978**, *11*, 607. Yamagishi, A.; Szwarc, M. *Macromolecules* **1978**, *11*, 504, 1091.
(6) Duda, A.; Penczek, S. *Macromolecules* **1994**, *27*, 4876. For example, this reference states that "one obtains the aggregation degree directly from the slope of the resulting straight line", i.e., from the log−log plot of R_p/[M] vs total active center concentration.
(7) Weiss, E. *Angew. Chem.* **1993**, *105*, 1565; *Angew. Chem., Int. Ed. Engl.* **1993**, *32*, 1501.
(8) Lambert, C.; Schleyer, P. v. R. *Angew. Chem.* **1994**, *106*, 1187; *Angew. Chem., Int. Ed. Engl.* **1994**, *33*, 1129.
(9) See, e.g.: *Developments in Ionic Polymers*; Wilson, A. D., Prosser, H. J., Eds.; Applied Science: London, 1983; Vol. 1. Dudevani, I.; Argawal, P. K.; Lundberg, R. D. *Polym. Eng. Sci.* **1982**, *22*, 499. MacKnight, W. J.; Earnest, T. R. *J. Polym. Sci. Macromol. Rev.* **1981**, *16*, 41.
(10) Morton, M.; Fetters, L. J. *Rubber Chem. Technol.* **1975**, *48*, 359.
(11) Berne, B. J.; Pecora, R. *Dynamic Light Scattering*; Wiley: New York, 1976.
(12) Provencher, S. *Makromol. Chem.* **1979**, *180*, 201.
(13) Fetters, L. J.; Hadjichristidis, N.; Lindner, J. S.; Mays, J. W. *J. Phys. Chem. Ref. Data* **1994**, *23*, 619.
(14) Bauer, B. J.; Fetters, L. J.; Graessley, W. W.; Hadjichristidis, N.; Quack, G. F. *Macromolecules* **1989**, *22*, 2337. R_G(star) = R_G(span)0.881$f_w^{0.187}$, where R_G(span) corresponds to the dimer. This expression is valid for the f_w range 2−32.
(15) Grest, G. *Macromolecules* **1994**, *27*, 3493.
(16) Willner, L.; Jucknischke, O.; Richter, D.; Roovers, J.; Zhou, L.-L.; Toporowski, P.; Fetters, L. J.; Huang, J.; Lin, M. Y.; Hadjichristidis, N. *Macromolecules* **1994**, *27*, 3821.
(17) Huber, K.; Burchard, W.; Fetters, L. J. *Macromolecules* **1984**, *17*, 541.
(18) Huber, K.; Bantel, S.; Burchard, W.; Fetters, L. J. *Macromolecules* **1986**, *19*, 1404.
(19) Richter, D.; Stühn, B.; Ewen, B.; Nerger, D. *Phys. Rev. Lett.* **1987**, *58*, 2462.
(20) Huber, K.; Bantle, S.; Lutz, P.; Burchard, W. *Macromolecules* **1985**, *16*, 1461.
(21) Leibler, L.; Orland, H.; Wheeler, J. C. *J. Chem. Phys.* **1983**, *79*, 3550.
(22) Balsara, N. P.; Tirrell, M.; Lodge, T. P. *Macromolecules* **1991**, *24*, 1975.
(23) Tauton, H. J.; Toprakcioglu, C.; Klein, J. *Macromolecules* **1988**, *21*, 3333.
(24) Tauton, H. J.; Toprakcioglu, C.; Fetters, L. J.; Klein, J. *Macromolecules* **1990**, *23*, 571.
(25) Klein, J.; Kumacheva, E.; Mahalu, D.; Perahia, D.; Fetters, L. J. *Nature* **1994**, *370*, 634.
(26) Perrin, F. *J. Phys. Rad.* **1934**, *5*, 497.
(27) Perrin, F. *J. Phys. Rad.* **1936**, *7*, 1.
(28) Kerker, M. *The Scattering of Light*; Academic Press: New York, 1969.
(29) Broersma, S. *J. Chem. Phys.* **1960**, *32*, 1626.
(30) Broersma, S. *J. Chem. Phys.* **1960**, *32*, 1632.
(31) Newman, J.; Swinney, H. L.; Day, L. A. *J. Mol. Biol.* **1977**, *116*, 593.
(32) Zhao, J. Q.; Pearce, E. M.; Kwei, T. K.; Jeon, H. S.; Kesani, P. K.; Balsara, N. P. *Macromolecules* **1995**, *28*, 1972.
(33) Jalal, N.; Duplessix, R. *J. Phys. Fr.* **1988**, *49*, 1775.
(34) Missel, P. J.; Mazer, N. A.; Benedek, G. B.; Young, C. Y.; Carey, M. C. *J. Phys. Chem.* **1980**, *84*, 1044. See also: Mazer, N. R.; Benedek, G. B.; Carey, M. C. *J. Phys. Chem.* **1976**, *80*, 1075.
(35) Puvvada, S.; Blankschtein, D. *J. Phys. Chem.* **1992**, *96*, 5579. See also: Puvvada, S.; Blankschtein, D. *J. Phys. Chem.* **1992**, *96*, 5567.
(36) Candau, S. J.; Hirsch, E.; Zana, R. *J. Colloid Interface Sci.* **1985**, *105*, 521. See also: Imae, T.; Ikeda, S. *J. Colloid Interface Sci.* **1984**, *99*, 300.
(37) Safran, S.; Turkevich, L. A.; Pincus, P. A. *J. Phys. Lett.* **1984**, *45*, L-69. See also: Israelachvilli, J. N.; Mitchell, D. J.; Ninham, B. W. *J. Chem. Soc., Faraday Trans. 2* **1976**, *72*, 1525.
(38) West, P.; Purmot, J. I.; McKinley, S. V. *J. Am. Chem. Soc.* **1968**, *90*, 797.
(39) Brubaker, G. R.; Beak, P. *J. Organomet. Chem.* **1977**, *136*, 147.
(40) Schümann, U.; Weiss, E.; Dietrich, H.; Mahdi, W. *J. Organomet. Chem.* **1987**, *332*, 229.
(41) Boche, G.; Etzrodt, H.; Marsch, M.; Massa, W.; Baum, H.; Dietrich, H.; Mahdi, W. *Angew. Chem.* **1986**, *98*, 84.
(42) Koster, H.; Weiss, E. *Chem. Ber.* **1982**, *115*, 3422.

(43) Winchester, W. R.; Bauer, W.; Schleyer, P. v. R. *J. Chem. Soc., Chem. Commun.* **1987**, 177.
(44) Atwood, J. L.; Fjeldberg, T.; Lappert, M. F.; Luong-Thi, N. T.; Shakir, R.; Thorne, A. J. *J. Chem. Soc., Chem. Commun.* **1984**, 1163.
(45) Halasa, A. F.; Mochel, V. D.; Fraenkel, G. In *Anionic Polymerization: Kinetics, Mechanisms and Synthesis*; McGrath, J. E., Ed.; ACS Symposium Series 166; American Chemical Society, Washington, DC, 1981; p 367.
(46) Brédas, J. L.; Chance, R. R.; Silbey, R. *Macromolecules* **1988**, *21*, 1633.
(47) Hommes, N. J. R. v. E.; Buhl, M.; Schleyer, P. v. R. *J. Organomet. Chem.* **1991**, *409*, 307. Note that 1 Hartree = 2.64×10^3 kJ.
(48) Jemmis, E. D.; Schleyer, P. v. R.; Pople, J. A. *J. Organomet. Chem.* **1978**, *154*, 325.
(49) Kaufmann, E.; Raghavachari, K.; Reed, A. E.; Schleyer, P. v. R. *Organometallics* **1988**, *7*, 1597.
(50) Graham, G.; Richtsmeier, S.; Dixon, D. A. *J. Am. Chem. Soc.* **1980**, *102*, 4572.
(51) By comparison, the presumed active center dissociation enthalpies of 38 kJ (ref 74, p 165; ref 76, p 63; and ref 82) and 50 kJ (ref 63, p 117) are equivalent to that, 42 ± 5 kJ, found for hydrogen-bonded polystyrene dimers; see Table 2 in: Merkle, G.; Burchard, W. *J. Phys. Chem.* **1992**, *96*, 3915. The 42 kJ value allows ~90% (20 °C) dissociation at an association site concentration of 10^{-5} M^{-1}. The butadienyllithium head group shows no detectable dissociation under similar conditions. See Table 2 of ref 4.
(52) Brown, T. L. *J. Organomet. Chem.* **1965**, *3*, 365.
(53) Schleyer, P. v. R. *Pure Appl. Chem.* **1984**, *56*, 151.
(54) Wilkinson, F. *Chemical Kinetics and Reaction Mechanisms*; Van Nostrand-Reinhold Co.: New York, 1980.
(55) Brown, T. L. *Adv. Organomet. Chem.* **1965**, *3*, 365.
(56) Johnson, A. F.; Worsfold, D. J. *J. Polym. Sci., Part A* **1965**, *3*, 449.
(57) Spirin, Yu. L.; Polykov, D. K.; Gantmakher, A. R.; Medvedev, S. *Dokl. Akad. Nauk SSSR* **1961**, *139*, 899.
(58) Fellers, J. F. Ph.D. Thesis, University of Akron, 1967.
(59) Gebert, W.; Hinz, J.; Sinn, H. *Makromol. Chem.* **1971**, *144*, 97.
(60) Ohlinger, R.; Bandermann, F. *Makromol. Chem.* **1980**, *181*, 1935.
(61) Johnson, A. F.; Worsfold, D. J. *Makromol. Chem.* **1965**, *85*, 273.
(62) Alvarino, J. M.; Bello, A.; Guzman, G. M. *Eur. Polym. J.* **1972**, *8*, 53.
(63) Bywater, S.; Worsfold, D. J. In *Recent Advances in Anionic Polymerization*; Hogen-Esch, T. E., Smid, J., Eds.; Elsevier: New York, 1987; p 109.
(64) Sinn, H.; Lundborg, C.; Onsager, O. T. *Makromol. Chem.* **1964**, *70*, 222.
(65) Guyot, A.; Vialle, J. *J. Macromol. Sci., Chem.* **1970**, *A4*, 107.
(66) Worsfold, D. J.; Bywater, S. *Can. J. Chem.* **1964**, *42*, 4884.
(67) Madani, E.; Favier, J. C.; Hemery, P.; Sigwalt, P. *Macromol. Chem., Rapid Commun.* **1990**, *11*, 329.
(68) Worsfold, D. J. *J. Polym. Sci., Polym. Chem. Ed.* **1967**, *5*, 2783.
(69) Spirin, Yu L.; Gantmakher, A. R.; Medvedev, S. S. *Dokl. Akad.* **1962**, *146*, 368.
(70) Helary, G.; Fontanile, M. *Eur. Polym. J.* **1978**, *14*, 345.
(71) Worsfold, D. J.; Bywater, S. *Can. J. Chem.* **1960**, *38*, 1981.
(72) Geerts, J.; van Beylen, M.; Smets, G. *J. Polym. Sci., Polym. Chem. Ed.* **1969**, *7*, 2859. Vacuum viscometry yields an $N_w \simeq 1.9$ for the (*o*-methoxystyryl)lithium head group at 0 and 20 °C. The reaction order of 0.62 at 20 °C (Table 3) dictates an apparent $N_n = 1.61$ or $N_w = 1.76$. N_w and N_n denote the weight and number average association states. The disparity in N_w values would be more pronounced at the lower temperatures: $N_w = 3 - 2N_n^{-1}$. The near constancy of N_w relative to temperature indicates that intramolecular solvation of the chain ends by the methoxy group does not significantly alter the association state.
(73) An evaluation of A_2 for the terminated polyisoprene chain ($M_w = 1.8 \times 10^4$ g mol^{-1}) of Figure 1 of ref 4 yields a value of 4.7×10^{-3} cm^3 mol g^{-2}, while the calculated value,[13] is 1.4×10^{-3} cm^3 mol g^{-2}. This disparity is outside typical experimental uncertainty.
(74) Szwarc, M.; van Beylen, M. *Ionic Polymerization and Living Polymers*; Chapman and Hall: London, 1993.
(75) Szwarc, M. *Carbanions, Living Polymers and Electron Transfer Processes*; Wiley: New York, 1968.
(76) Szwarc, M. *Adv. Polym. Sci.* **1983**, *49*, 1.
(77) Szwarc, M. In *Recent Advances in Anionic Polymerization*; Hogen-Esch, T. E., Smid, J., Eds.; Elsevier: Dordrecht 1987; p 93.
(78) Bywater, S. *Prog. Polym. Sci.* **1974**, *4*, 27.
(79) Szwarc, M. *Makromol. Chem., Macromol. Symp.* **1993**, *67*, 83.
(80) Szwarc, M. *Kobunshi* **1991**, *40*, 798.
(81) Szwarc, M. In *Macromolecules, Main Lectures, 27th International Symposium (IUPAC)*; Benoit, H., Rempp, P., Eds.; Pergamon Press: Oxford, U.K., 1982; p 15.
(82) Szwarc, M. *J. Polym. Sci., Polym. Lett. Ed.* **1980**, *18*, 493.
(83) Müller, A. E. H. In *Comprehensive Polymer Science*; Eastmond, G. C.; Ledwith, A., Russo, S., Sigwalt, P., Eds.; Pergamon Press: Oxford, U.K., 1989; p 357.
(84) Szwarc, M. In *Anionic Polymerization: Kinetics Mechanisms and Synthesis*; McGrath, J. E., Ed.; ACS Symposium Series 166; American Chemical Society: Washington, DC, 1981; p 1.
(85) Bywater, S. *Prog. Polym. Sci.* **1994**, *19*, 287.
(86) Young, R. N.; Fetters, L. J.; Huang, J.; Krishnamoorti, R. *Polym. Int.* **1994**, *33*, 217.
(87) Smart, J. B.; Hogan, R.; Scherr, P. A.; Emerson, M. T.; Oliver, J. P. *J. Organomet. Chem.* **1974**, *64*, 1. This reference advocates a mechanism involving direct reaction with organolithium aggregates which can account for the cis and trans structures in polydienes.
(88) Shamanin, V. V.; Melenevskaya, E. Yu.; Sgonnik, V. N. *Acta Polym.* **1982**, *33*, 175.
(89) Makowski, H. S.; Lynn, M. *J. Macromol. Chem.* **1966**, *1*, 443.
(90) Fetters, L. J.; Kiss, A. D.; Pearson, D. S.; Quack, G. F.; Vitus, F. J. *Macromolecules* **1993**, *26*, 647.
(91) Evidence is available[63,67] which shows that the chain molecular weight will influence propagation rates; i.e., an increase in chain length at constant head-group concentration increases the observed rate. This could be a reflection of the relative concentrations of dimers and the large scale structures responding to chain length.
(92) Dienyllithium head groups exist in both the cis and trans forms; e.g., see: Worsfold, D. J.; Bywater, S. *Macromolecules* **1978**, *11*, 582. Glaze, W. H.; Hanicak, J. E.; Moore, M. L.; Chaudhuri, J. *J. Organomet. Chem.* **1972**, *44*, 39.
(93) The vacuum viscometry method has yielded N_w of 2 irrespective of head-group identity; e.g., see: Morton, M.; Fetters, L. J.; Pett, R. A.; Meier, J. F. *Macromolecules* **1970**, *3*, 3273. Al-Jarrah, M. M.; Young, R. N. *Polymer* **1980**, *21*, 119. Szwarc, M.; Wang, H. C. *Macromolecules* **1982**, *15*, 208. See also ref 3. As Cates has concluded for pairwise associates, "measurements of viscosity can yield useful information ... so long as τ_{break}" (dimer lifetime) "is within an order of magnitude or two either side of T_d" (the disengagement time of a dissociated chain in its tube). The dissociation enthalpies previously mentioned require that the interplay of τ_{break} and T_d fulfills Cates scenario. Cates M. *Macromolecules* **1988**, *21*, 256.

MA950183N